CHAPTER 4

4.1 Synthesis of catalysts

4.1.1 Preparation of calcium oxide (CaO) catalyst from waste crab shells

Crab shells were collected from Jas Dry Fish Merchant-India MART Toothukudi, Tamil Nadu, India. Collected crab shells were washed entirely with distilled water to eliminate dust particles and impurities associated with the crab shells as shown in Figure 4.1. After washing with distilled water, crab shells were kept in hot air oven at 102 ℃ for 5 hours to remove water content present in the crab shells. Thereafter, crab shells were cut into small species and these small pieces were grounded into powder with the help of ball mill apparatus. This powder was calcined at different temperatures ranging from 450 ℃ to 850 ℃. Calcium carbonate ($CaCO_3$), present in the crab shells was converted into calcium oxide (CaO) when the temperature reached at 850 ℃ in a tubular furnace for 4 hours. The calcined material was powdered in agate mortar and kept in desiccators to avoid moisture, further used as efficient solid base catalyst in transesterification reaction for the synthesis of biodiesel from waste fish oil. The prepared calcium oxide was highly stable and was able to hold its catalytic activity to the transesterification reactions [Boey et al., 2011a]. Prepared catalyst was characterized with various techniques such as XRD, FT-IR, TG/DTA/DTG and SEM/EDX.

Figure 4.1 Represents the collected waste crab shells.

4.1.2 Characterization of synthesized calcium oxide

4.1.2.1 X-ray diffraction patterns (XRD)

Figure 4.2 represents the X-ray diffraction patterns of the calcium oxide derived from waste crab shells. Synthesized samples were characterized with XRD in the 2θ range of 20° – 80° at the step rate of 0.4θ/s. All the diffracted peaks obtained from the XRD analysis were of characteristics of calcined waste crab shells at different temperatures varied from 450 °C to 850 °C for 4 hours. Calcination temperature plays a vital role in the process of conversion of calcium carbonate present in the waste crab shells into calcium oxide through decomposition. Calcium carbonate peaks were observed at ca. 23, 29.4, 36, 39.4, 43.1, 47.5 and 48.5 (JCPDS 85-1108) as the temperature was raised up to 450 °C. Calcium oxide peaks were observed when temperature was raised at

450 ℃ to 650 ℃ but along with calcium oxide peaks calcium carbonate peaks also observed due to incomplete decomposition of calcium carbonate. Pure and stable calcium oxide was obtained upon calcination temperature at 850 ℃ for 4 hours and no calcium carbonate peaks were observed since at this temperature complete conversion of calcium carbonate present in waste crab shells were converted into calcium oxide. XRD peaks of calcined crab shells were observed at ca. 32, 37.3, 53.8, 64.4 and 67.3 and these peaks were matched with JCPDS 48-1467 which clearly indicated that the obtained compound upon calcination was calcium oxide.

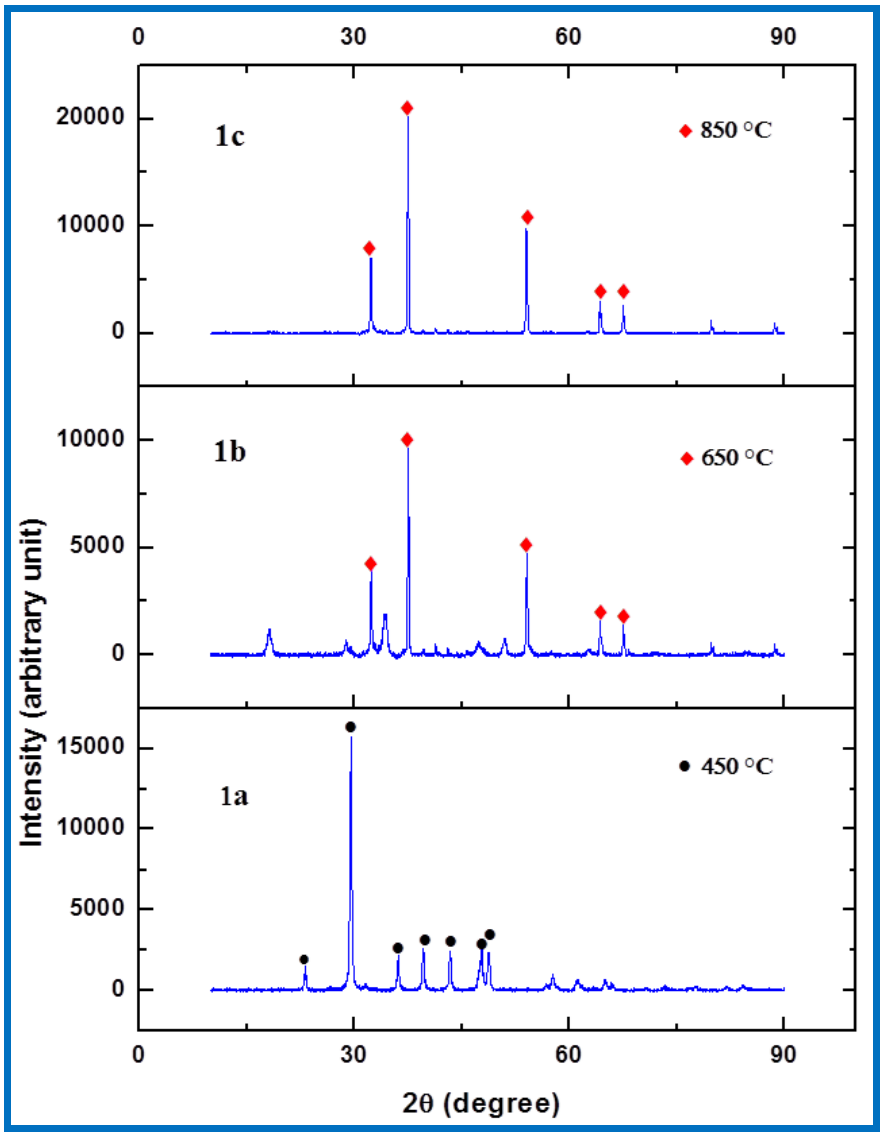

Figure 4.2 (1a) XRD patterns of calcined crab shell catalyst at 450 °C, (1b) represents the XRD patterns of calcined crab shell catalyst at 650 °C, (1c) represents the XRD patterns of calcined crab shell catalyst at 850 °C.

4.1.2.2 TG/DTA/DTG analysis

Thermal gravimetric analysis has been done to evaluate the decomposition temperature with respect to weight loss of the sample. 10.170 mg of uncalcined crab shell powder was

used for the analysis of TG/DTA/DTG. Considerable weight loss (5.41%) of the sample was observed in TG curve from room temperature 27°C to 230 °C and it was due to removal of water molecule. Effective weight loss (39.9 %) was observed from 600 °C to 785 °C due to decomposition of calcium carbonate into calcium oxide by releasing carbon dioxide and after that no further weight loss was observed as shown in the following equation (Eq. 4.1). The first derivative in DTA curve at 350 °C was due the decomposition of the calcium hydroxide ($Ca(OH)_2$) into calcium oxide (CaO) [Sharma et al., 2010]. No weight loss was observed when temperature was raised from 785 °C to 1100 °C; this clearly indicated that the complete conversion of calcium carbonate into calcium oxide occurred below 850 °C as shown in Figure 4.3.

$$CaCO_3 \rightarrow CaO + CO_2 \qquad (4.1)$$

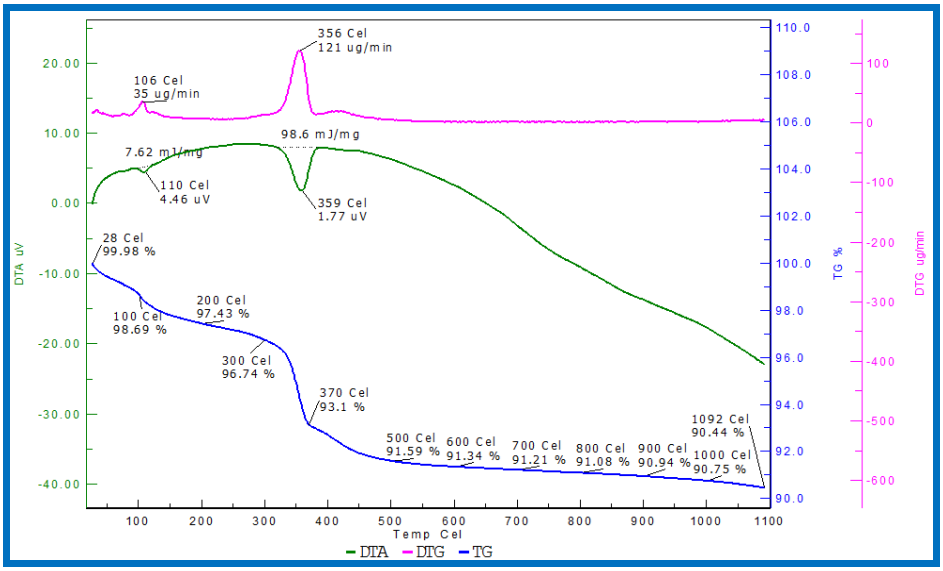

Figure 4.3 TG/DTA/DTG of uncalcined crab shells.

4.1.2.3 SEM/EDS analysis

The SEM (Scanning Electron Microscopy) image of calcium oxide (CaO) derived from waste crab shells has been depicted in Figure 4.4. It was observed from the figure that regular spear like morphology particles were present in calcium oxide (CaO) derived from waste crab shells. It is clearly observed that the no overlapping of particles was present and the size range from 1.80 to 2.60 µm of width was observed but large number of particles were in 2.02 to 2.34 µm range. Elemental analysis of calcium oxide (CaO) derived from waste crab shells was performed by Energy Dispersive X-ray Spectroscopy (Figure 4.5), which clearly specified the presence of calcium (weight % was 53.21 and atomic % was 31.22) and oxygen (weight % was 46.79 and atomic % was 68.78) due to the complete conversion of calcium carbonate ($CaCO_3$) into calcium oxide (CaO) upon calcination as shown in Table 4.1.

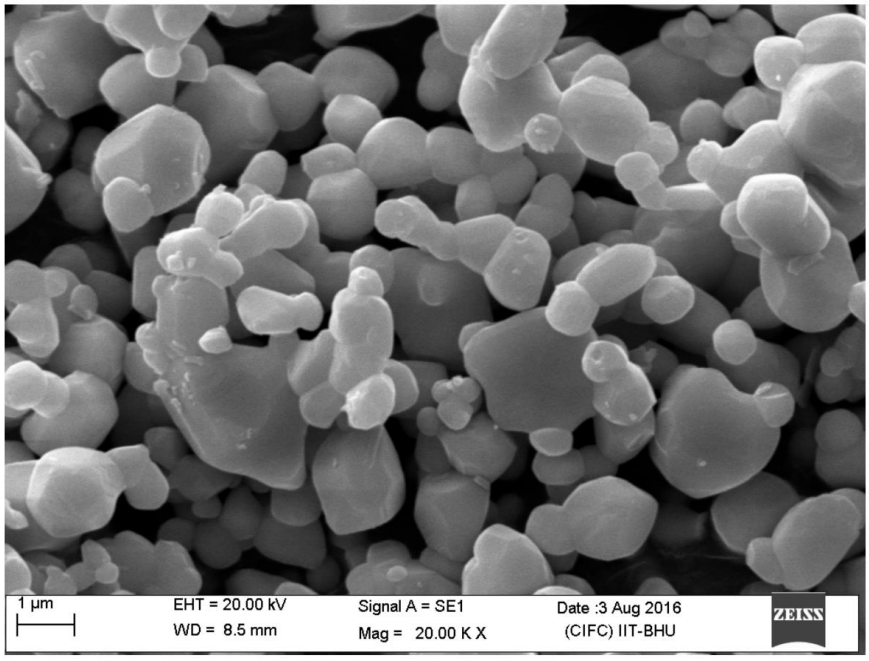

Figure 4.4 Represents the SEM of calcium oxide derived from waste crab shells.

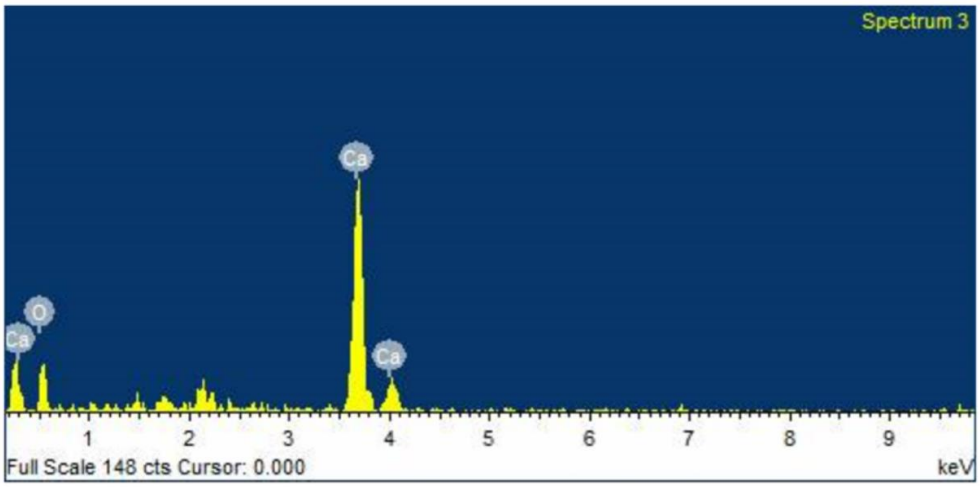

Figure 4.5 Represents the EDX spectrum of calcium oxide derived from waste crab shells.

Table 4.1 Elemental composition of calcium oxide (weight % and atomic %) by EDX analysis.

Element	Weight %	Atomic %
O	46.79	68.78
Ca	53.21	31.22
Total	100.00	

4.1.2.4 FT-IR analysis

Figure 4.6 represents the Fourier Transform Infrared Spectroscopy (FT-IR) of calcium oxide (CaO) derived from waste crab shells upon calcination at different temperatures. The sharp and intense infrared band observed at 507 cm^{-1} is a characteristic of Ca-O stretching vibration mode. Complete conversion of calcium carbonate ($CaCO_3$)

into calcium oxide (CaO) when the calcination temperature raised from 650 °C to 850 °C because no carbonyl group (C=O) infrared bands were observed and vibration band occurred at 2352 cm^{-1}, and this evidently specifies the existence of gaseous CO_2. Sharp stretching band was observed at 3625 cm^{-1} for the catalyst calcined at 850 °C, was due to the presence –OH group of water molecule on the surface of calcium oxide catalyst derived from waste crab shells.

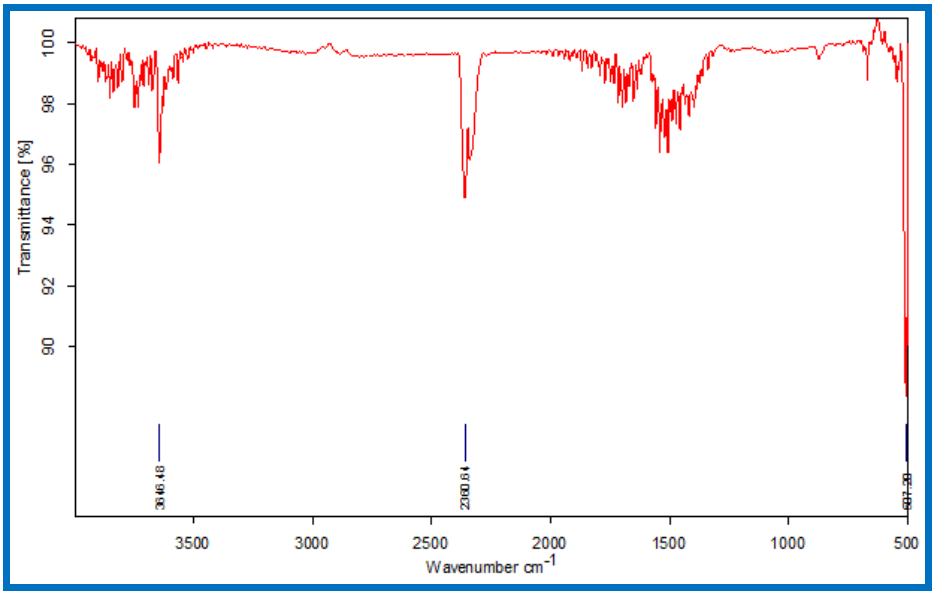

Figure 4.6 FT-IR spectrum of calcium oxide derived from waste crab shells.

4.1.3 Preparation of β-tri-calcium phosphate ($Ca_3(PO_4)_2$) catalyst from waste parts of fish

Fish oil was extracted from waste parts of fish through the mechanical expeller followed by solvent extraction. After extraction of waste fish oil from waste parts of fish, solid matter was left which included fish bones, tails, fins etc. This solid matter was

washed several times with hot distilled water to remove fat, flesh and gelatinous material associated with solid matter. Thereafter, solid matter was kept in hot air oven at 102 ℃ for 5 hours to remove water content present in the solid matter. The dried solid matter was ground into powder with the help of ball mill, further powder was calcined in a muffle furnace at different temperature ranging from 400 ℃ to 1000 ℃ for 4 hours. The calcined substance was grounded into fine powder with the help of agate mortar and characterized with different analytical techniques such as TG/DTA/DTG, FT-IR XRD and SEM/EDX.

4.1.3.1 XRD Patterns of β-tricalcium phosphate

Figure 4.7 represents the XRD diffraction spectra of calcined solid matter over a temperature range from 400 °C to 1000 °C. Solid matter comprises naturally occurring hydroxyapatite in the form of calcium apatite mineral with formula ($Ca_5(PO_4)_3$) but to represents the crystal unit cell, it can be written as $Ca_{10}(PO_4)_6(OH)_2$. XRD pattern of solid matter contains hydroxyapatite ($Ca_{10}(PO_4)_6(OH)_2$) converted into β-tricalcium phosphate ($Ca_3(PO_4)_2$) as the calcination temperature was raised from 600 °C to 800 °C but at 800 °C, both forms (hydroxyapatite ($Ca_{10}(PO_4)_6(OH)_2$) and β-tricalcium phosphate ($Ca_3(PO_4)_2$) existed. Highly intense and narrow peaks in XRD of solid matter calcined at 1000 °C indicated the major portion of β-tricalcium phosphate than the hydroxyapatite and the prominent peaks of β-tricalcium phosphate observed according to JCPDS file (70-2065) were at ca. 21.8, 26.4, 31.02, 34.3, 39.8, 46.9 and 51.4.

Negligible percentage of hydroxyapatite peaks were observed in XRD of solid matter calcined at 1000 °C according to JCPDS file (74-0565) at ca. 28.9, 32.8 and 49.4.

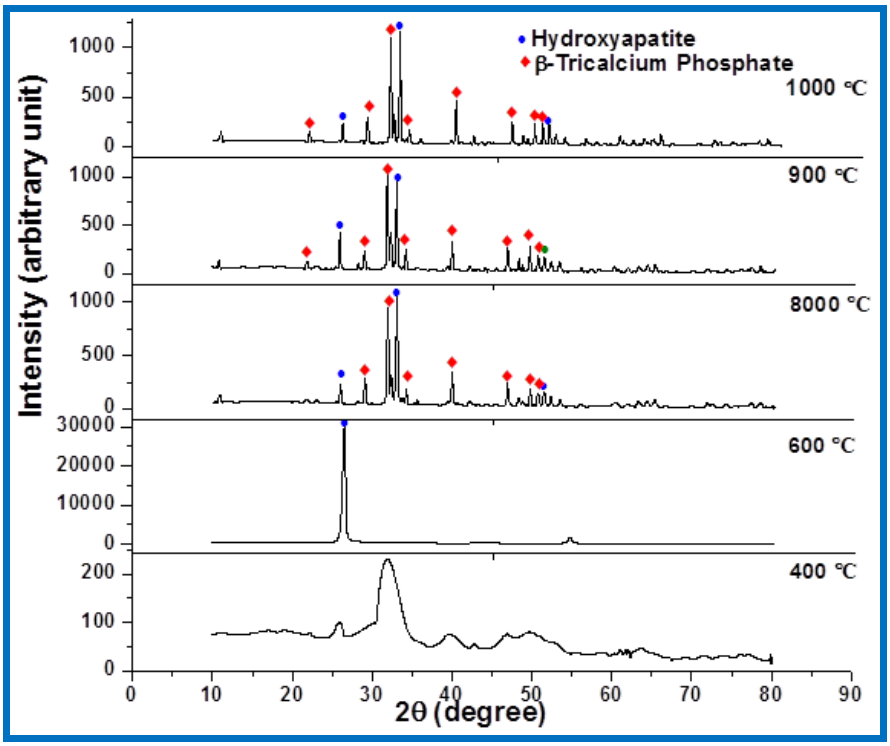

Figure 4.7 Diffractogram of (a) β-Tri-calcium Phosphate (b) Hydroxyapatite

4.1.3.2 TG/DTA/DTG analysis of solid matter

Figure 4.8 represents the thermo-gravimetric analysis (TG/DTA/DTG) uncalcined solid matter. 10.200 mg of uncalcined solid matter was taken to study the TG/DTA/DTG analysis. The weight loss of uncalcined solid matter was observed in the temperature range from 35 °C to 1200 °C with the increment of 10 °C/min. The total weight loss of

uncalcined solid matter in TG curve was found to be 43.48 %. Sharp weight loss, nearly 10.05 % occurred in TG curve at 35 °C < T < 200 °C, was due to the release of the adsorbed water and lattice form of water present in the solid matter. High weight loss observed at 200 °C < T < 600 °C was corresponding to the release of lattice water present as well as organic matter such collagen, lipids, chondroitin sulfate, and keratin sulfate [Tada, 1975] present in the solid matter. Insignificant weight loss observed at 600 °C < T < 900 °C was due the release of some amount residual organic matter present in the solid matter. No significant weight loss was observed at a temperature lesser than 900 °C since the conversion of β-tricalcium phosphate from hydroxyapatite was occurred [Venkatesan and Kim, 2010], further temperature was raised up to 1000 °C but no significant weight loss was seen in TGA curve which indicates the high thermal stability of β-tricalcium phosphate. Differential Thermal Analysis (DTA) and Derivative Thermogravimetric analysis (DTG) helped in finding the temperature at which organic matter was released from solid matter. Two exothermic peaks in DTG curve were corresponding to two weight losses and minor endothermic heat exchange in DTA curve at T > 800 °C, which could be lattice rearrangements and apatite crystallization.

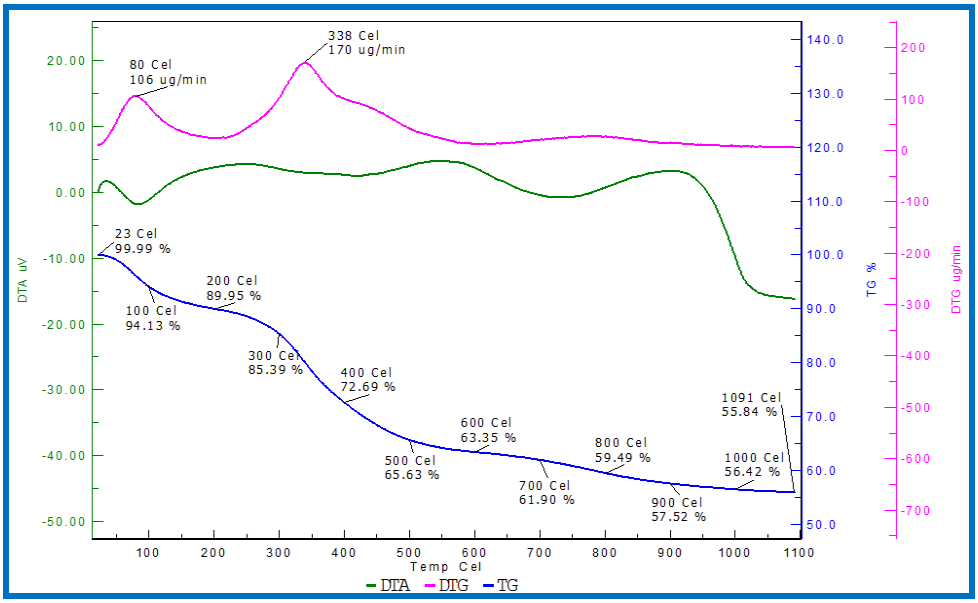

Figure 4.8 Thermo-gravimetric analysis (TG/DTA/DTG) of solid matter

4.1.3.3 FT-IR analysis

Fourier transform infrared spectroscopy (FT-IR) is well known analytical method to identify the functional groups present in a compound. The sharp vibration band occurred at 560 cm^{-1} ascribed the presence of PO_4^{3-} functional group present in the prepared catalyst [Chen et al., 2008]. The broad peak at 1644 cm^{-1} indicated to absorbed water from the atmosphere and sharp vibration peak observed at 962 cm^{-1} was corresponding to PO_4^{3-} [Tanaka et al., 2012]. The absorption bands at 962 cm^{-1} and 1087 cm^{-1} were attributed to hydroxyapatite [Filgueiras et al., 1993] since minor amount of hydroxyapatite present along with the β-tricalcium phosphate as shown in Figure 4.9.

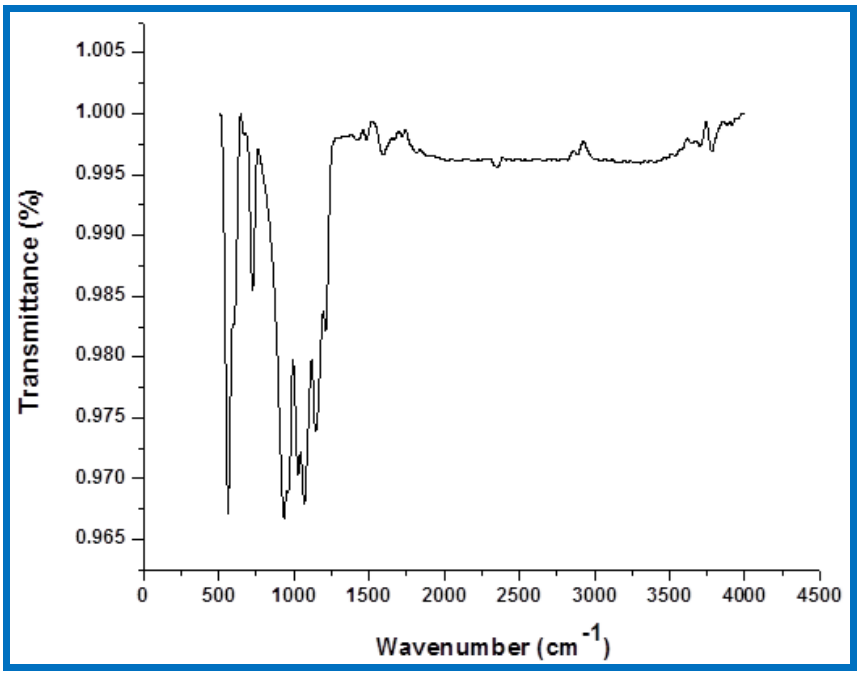

Figure 4.9 FT-IR spectrum of β-tricalcium phosphate.

4.1.3.4 SEM/EDX analysis

Figure 4.10 represents the scanning electron spectroscopy of prepared catalyst. The surface morphology of β-tricalcium phosphate prepared from solid matter was porous and the particles were homogeneous with regular shapes. Effect of calcination temperature on surface of catalyst was clearly seen since the porous nature of β-tricalcium phosphate increased with increasing calcination temperature. Elemental composition of β-tricalcium phosphate was determined by using energy dispersive X-ray spectroscopy (EDX) as shown in Figure 4.11. The atomic percentages of phosphorus, oxygen and calcium were 19.34 %. 60.82 % and 19.85 % respectively as shown in Table 4.2. The EDX spectrum results showed that the weight percentages of phosphorus, oxygen and

calcium were 25.30 %, 41.10 % and 33.60 % respectively. The EDX results clearly indicated that the prepared catalyst had phosphorus (P), oxygen (O) and calcium (Ca).

Table 4.2 Elemental composition of β-tricalcium phosphate (weight % and atomic %).

Element	Weight %	Atomic %
O	41.10	60.82
P	25.30	19.34
Ca	33.60	19.85
Totals	100.00	

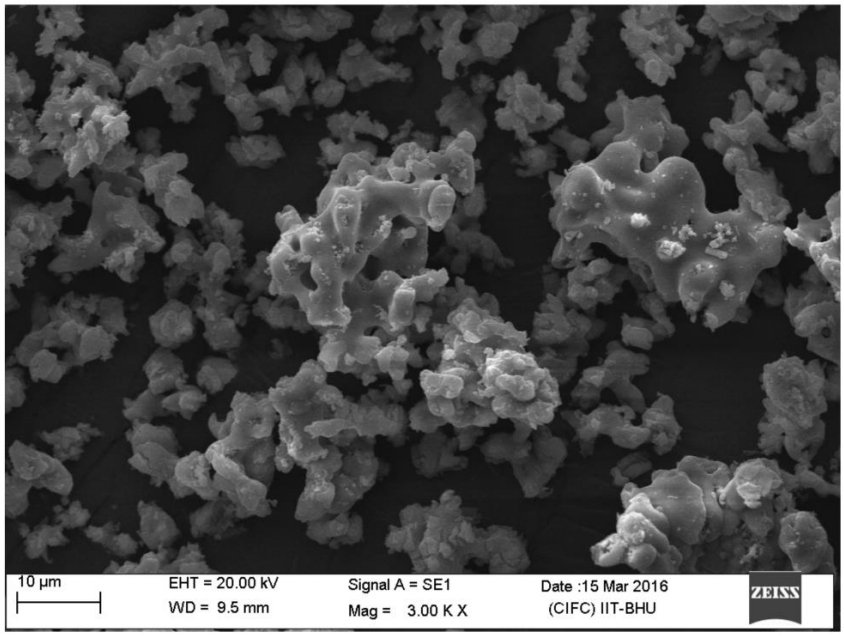

Figure 4.10 SEM of β-tricalcium phosphate base catalyst derived from waste fish bone.

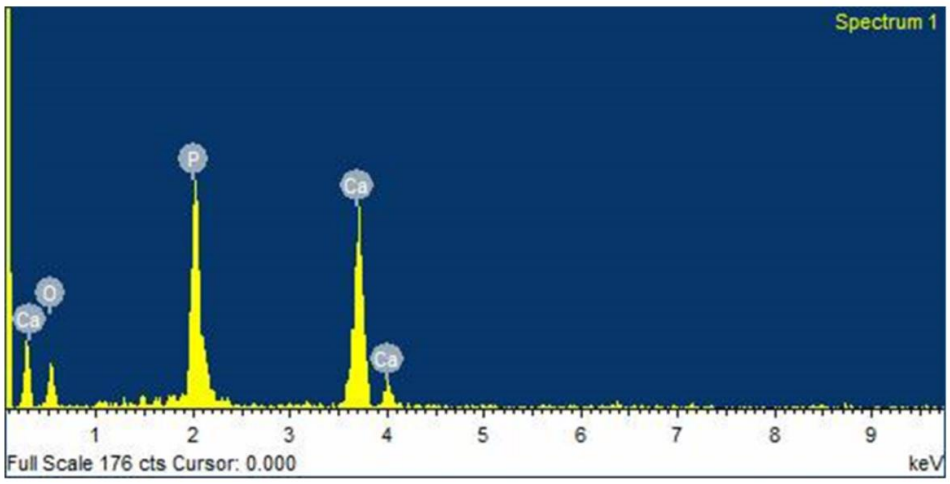

Figure 4.11 EDX spectrum of β-tricalcium phosphate.

4.2 *Pongamia pinnata* oil extraction

Pongamia pinnata oil extraction was carried out by using soxhlet apparatus through solvent extraction [Bhutada et al., 2016]. *Pongamia pinnata* seeds were collected from the local market in Varanasi, India and dried in hot air oven at 102 C° for 100 min to remove moisture as shown in Figure 4.12. Dried seeds were cut into small pieces and grinded into flour with the help of ball mill. *Pongamia pinnata* oil was extracted using this flour with different solvents viz. n-hexane, petroleum ether and dimethyl ether. Highest yield 43.73 % of *Pongamia pinnata* oil was observed in the case of petroleum ether and the lowest was yield was 38.92 % observed was in the case of n –hexane as shown in Table 4.3. Average ratio of flour to solvent was 5 g: 30 ml. In an average 20 g of *Pongamia pinnata* seeds gave 8 g oil, approximately 38 to 43% yield. Physical and chemical properties of

extracted *Pongamia pinnata* oil were determined and used as feedstock for the synthesis of biodiesel as shown in Table 4.4.

Figure 4.12 Represets the *Pongamia pinnata* seeds.

Table 4.3 Solvent extraction of *Pongamia pinnata* seeds using different solvents.

Solvent (10mL/g of seed)	Weight of seed (g)	Stirring time (hr.)	Weight of crude oil (g)	Yield of oil (%)
	10.03	2	4.2	41.87
Petroleum ether	10.05	3	4.3	42.78
	10.06	4	4.4	43.73
	10.02	2	3.9	38.92
Hexane	10.03	3	4.1	40.87
	10.06	4	4.2	41.74
	10.01	2	4.0	39.96
Diethyl ether	10.03	3	4.1	40.87
	10.06	4	4.3	42.74

Table 4.4 Physical and chemical properties of *Pongamia pinnata* oil.

Property	Unit	ASTM Standards	Value
Color	-		Yellowish red
Acid value	mg KOH/g	ASTM D 664	17.68
Unsaponifiable matter	% w/w		2.5
Density	g/cm^3	ASTM D 1298	0.934
Boiling point	°C	-	321
Cloud point	°C	ASTM D 1510	5
Saponification value	mg KOH/g		188
Pour point	°C	ASTM D 97	4
Kinematic viscosity(mm^2/s), at 40 °C	mm^2/s	ASTM D 445	39.3
Flash point	°C	ASTM D 93	214
Calorific value	kcal/kg	ASTM D 4809	8703
Water content	in %	ASTM D 2709	0.008%
Copper strip corrosion	3h/50 °C	ASTM D 130	No Corrosion observed

4.2.1 Characterization of *Pongamia pinnata* oil

4.2.1.1 Gas Chromatography–Mass Spectrometry (GC-MS) analysis of *Pongamia pinnata* oil

The method implemented to determine the fatty acid composition was esterification reaction (methanol as solvent and H_2SO_4 as homogeneous catalyst) followed by transesterification, where the fatty acid composition present in the *Pongamia pinnata*

oil get converted into corresponding methyl esters and these methyl esters were analysed with GC-MS. Sample was prepared with 0.03 mL of above oil (after esterification) mixed with 2.1 mL of hexane for the GC-MS analysis (Section 3.7.3, Chapter 3). Figure 4.13 represents the GC-MS chromatogram of *Pongamia pinnata* oil in which X-axis corresponds to retention time and Y-axis corresponds to percentage of relative abundance. Using the known compound spectrum from the NIST 2011 library, unknown compound spectrum was predicted with the help of Turbo Mass software. GC-MS analysis showed that the fatty acid composition present in the *Pongamia pinnata* oil were, Palmitic acid methyl ester (Figure 4.14), Oleic acid methyl ester (Figure 4.15), Stearic acid, methyl ester (Figure 4.16), cis – 11-Eicosenoic acid methyl ester (Figure 4.17), Arachidic acid methyl ester (Figure 4.18), Behenic acid, methyl ester (Figure 4.19) respectively. Table 4.5 depicts the fatty acid composition and their corresponding structures with retention time.

Table 4.5 Fatty acid composition (%) of *Pongamia pinnata* oil.

Sr.	Retention time	Compound name	Composition (%)	Corresponding fatty acid	Corresponding fatty acid structure
1	19.89	Palmitic acid methyl ester	10.41	Palmitic acid	$CH_3(CH_2)_{12}COOH$
2	21.75	Oleic acid methyl ester	66.30	Oleic acid	$CH_3(CH2)_{14}CH=CHCOOH$
3	21.89	Stearic acid methyl ester	9.07	Stearic acid	$CH_3(CH_2)_{16}COOH$
4	23.38	cis–11-Eicosenoic acid methyl ester	3.88	cis–11-Eicosenoic acid	$CH_3(CH_2)_{16}(CH=CH)COOH$
5	23.62	Arachidic acid methyl ester	5.09	Arachidic acid	$CH_3(CH_2)_{10}(CH=CH)_4COOH$
6	25.27	Behenic acid, methyl ester	4.02	Behenic acid	$CH_3(CH_2)_{20}COOH$

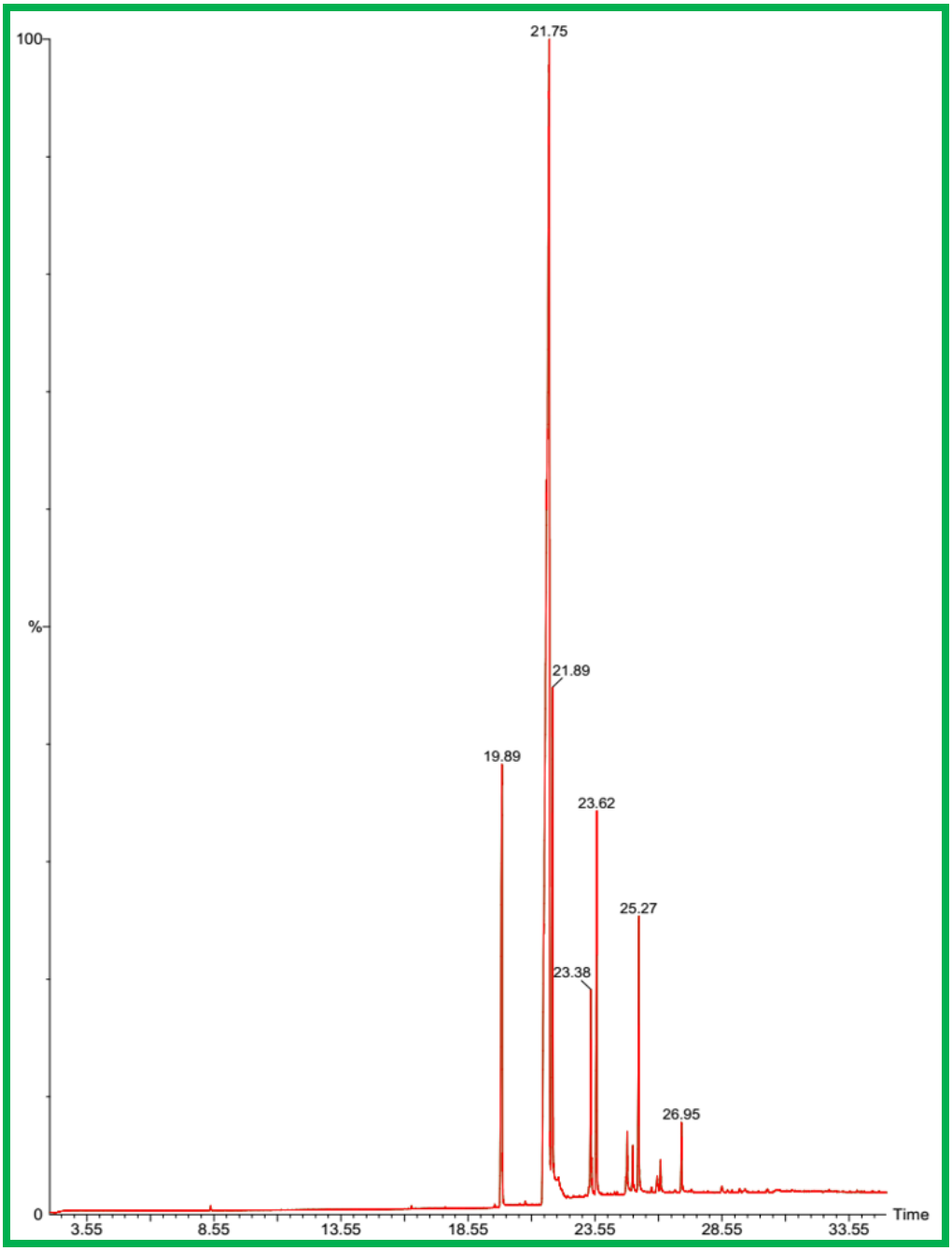

Figure 4.13 GC-MS chromatogram of *Pongamia pinnata* oil.

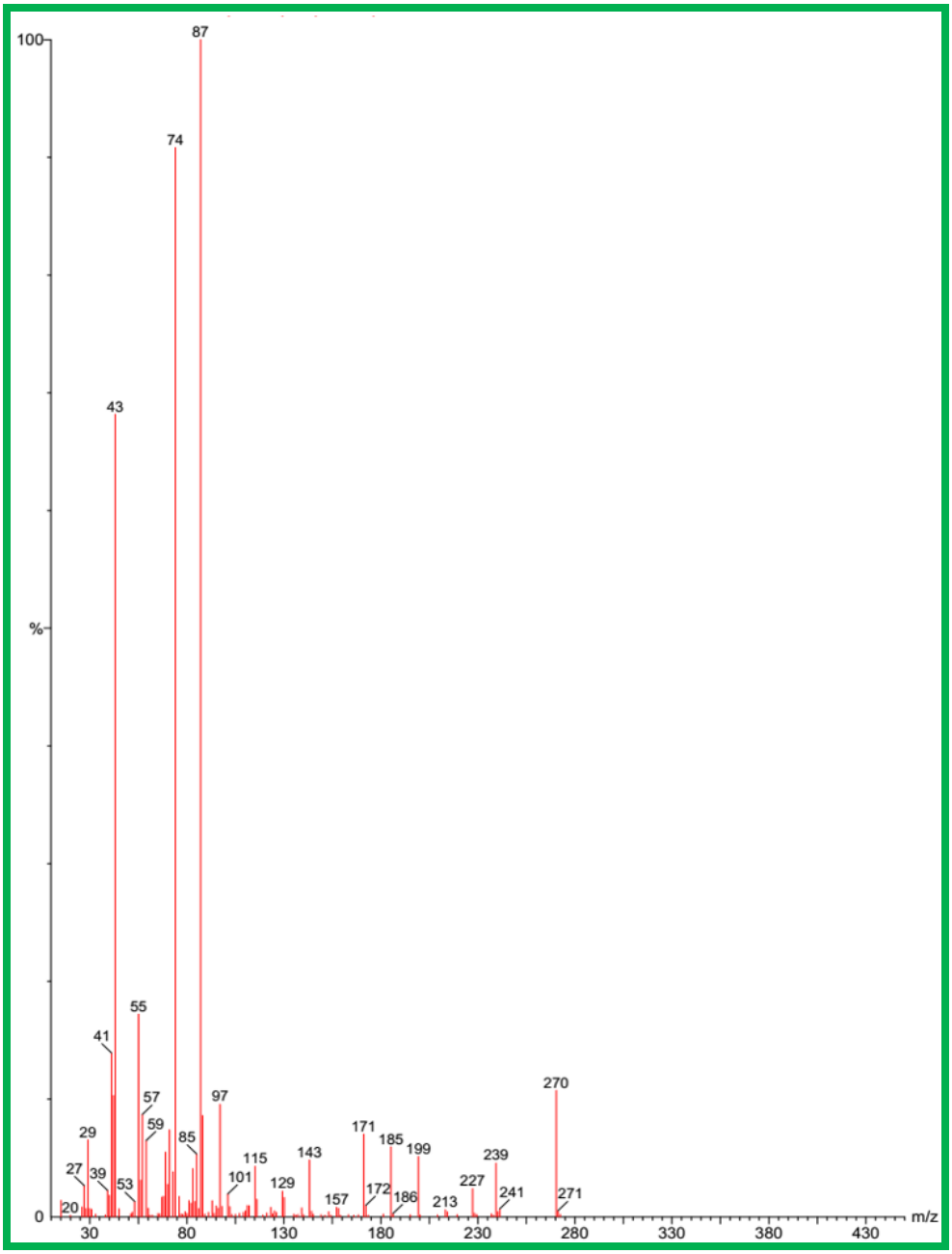

Figure 4.14 GC-MS spectrum of palmitic acid methyl ester

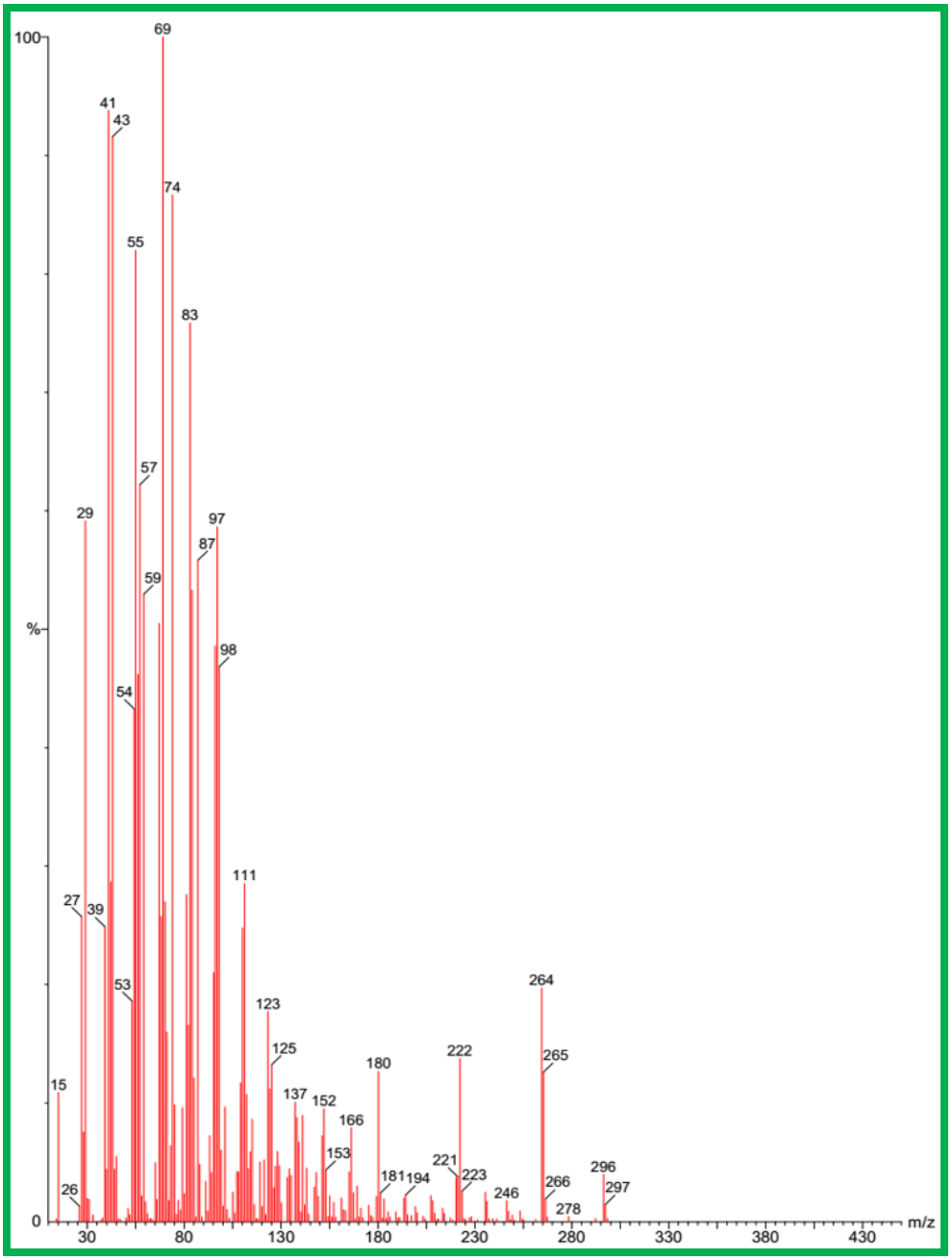

Figure 4.15 GC-MS spectrum of oleic acid methyl ester

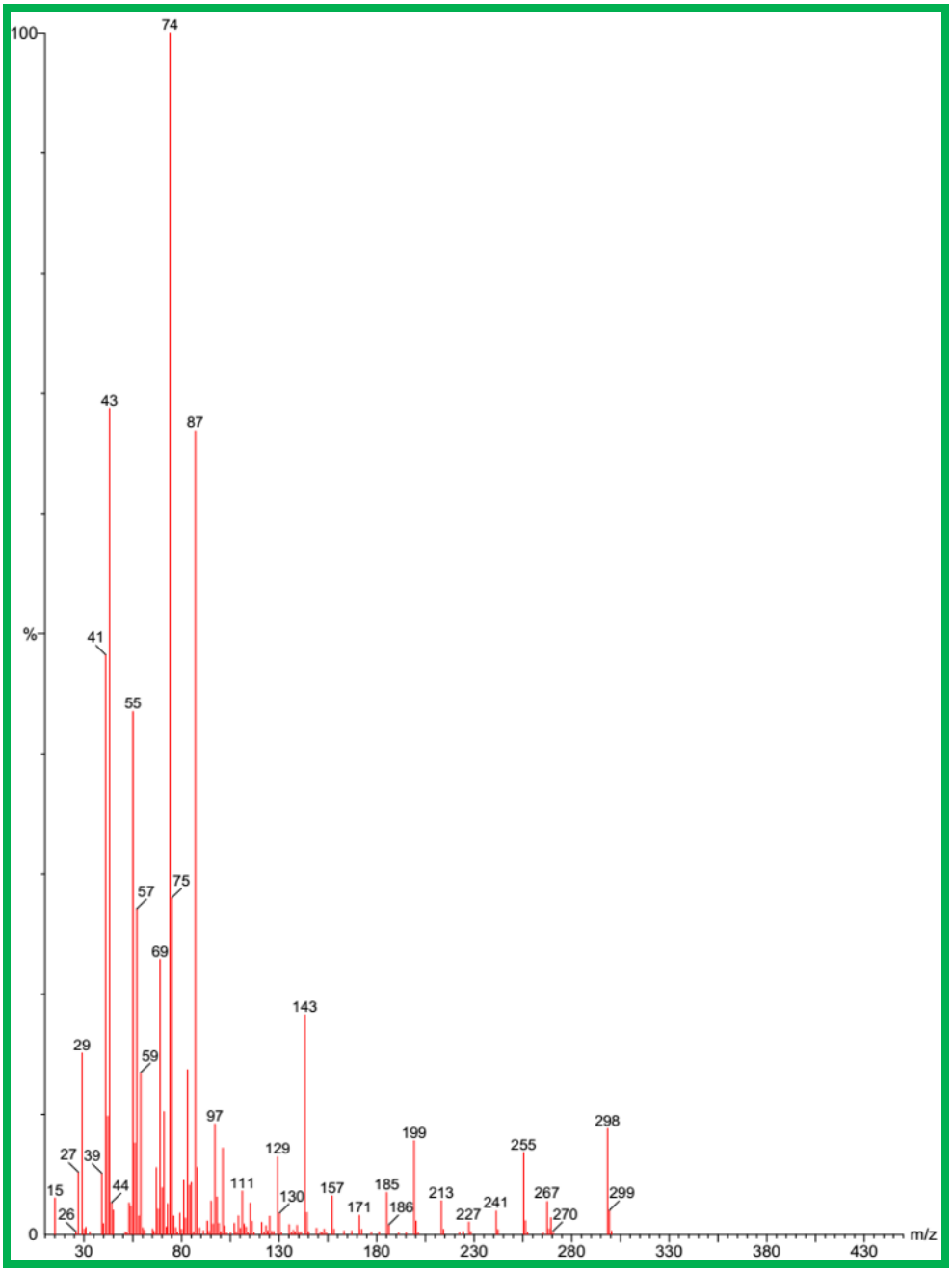

Figure 4.16 GC-MS spectrum of stearic acid, methyl ester

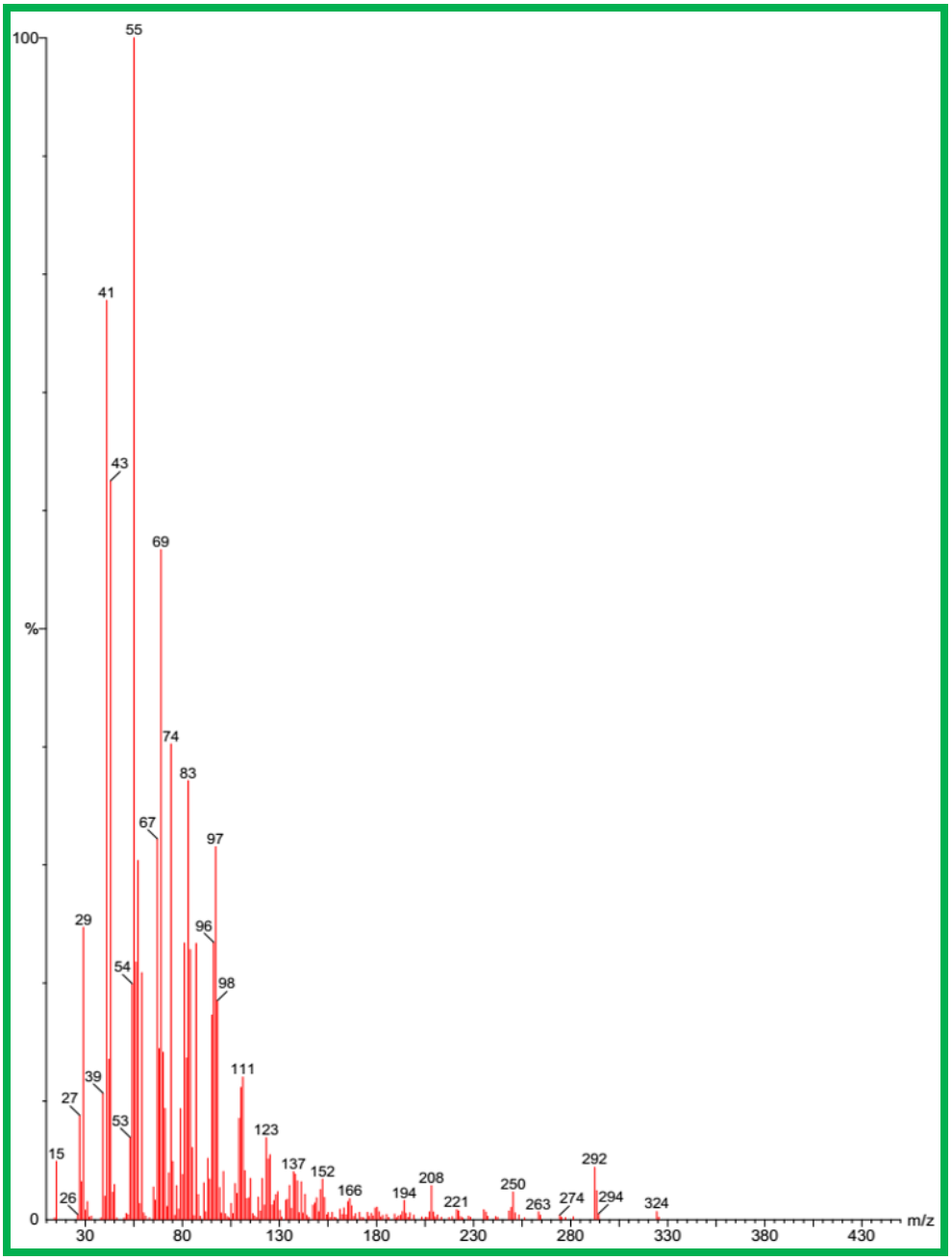

Figure 4.17 GC-MS spectrum of cis - 11- eicosenoic acid methyl ester

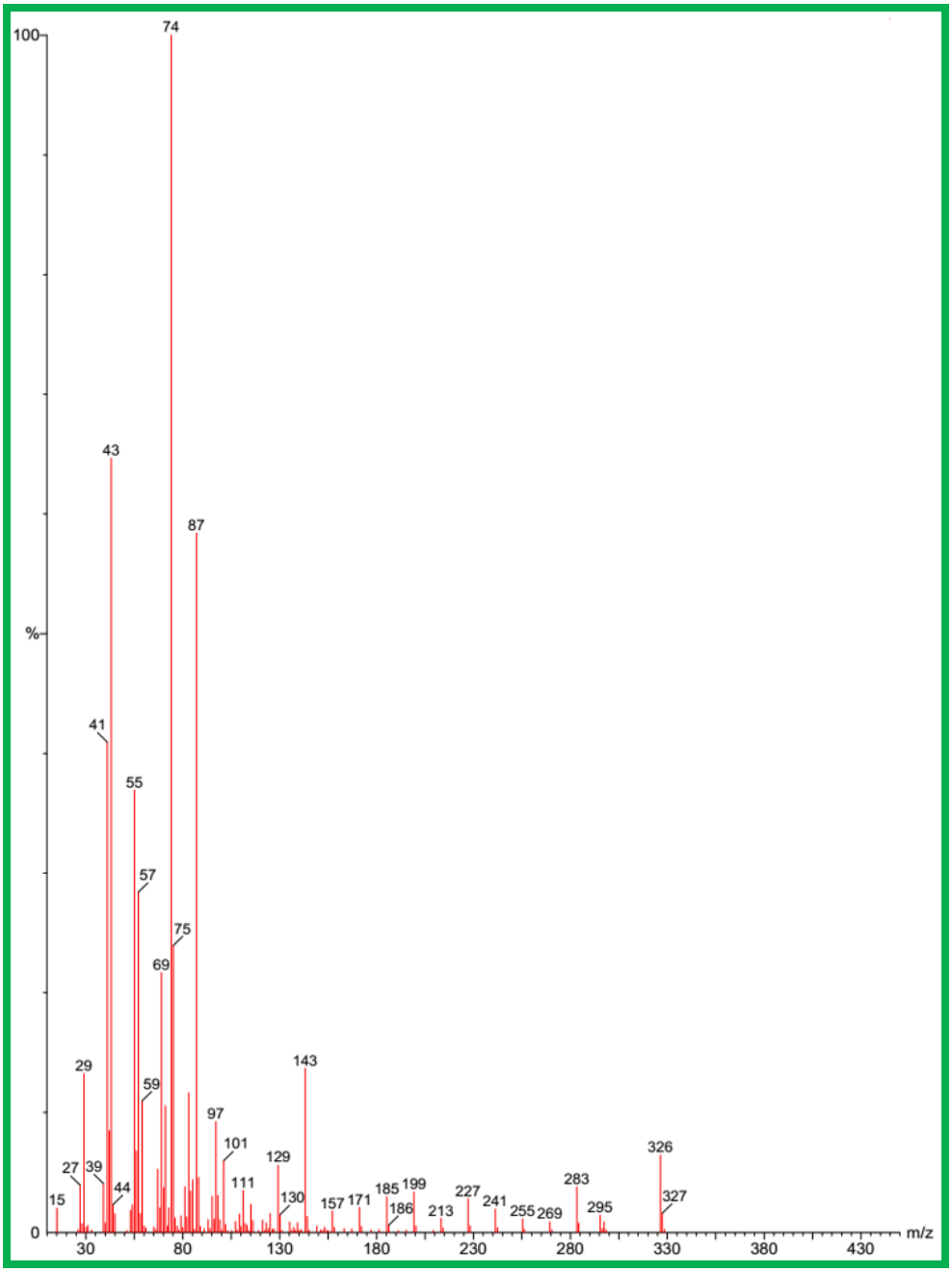

Figure 4.18 GC-MS spectrum of arachidic acid methyl ester

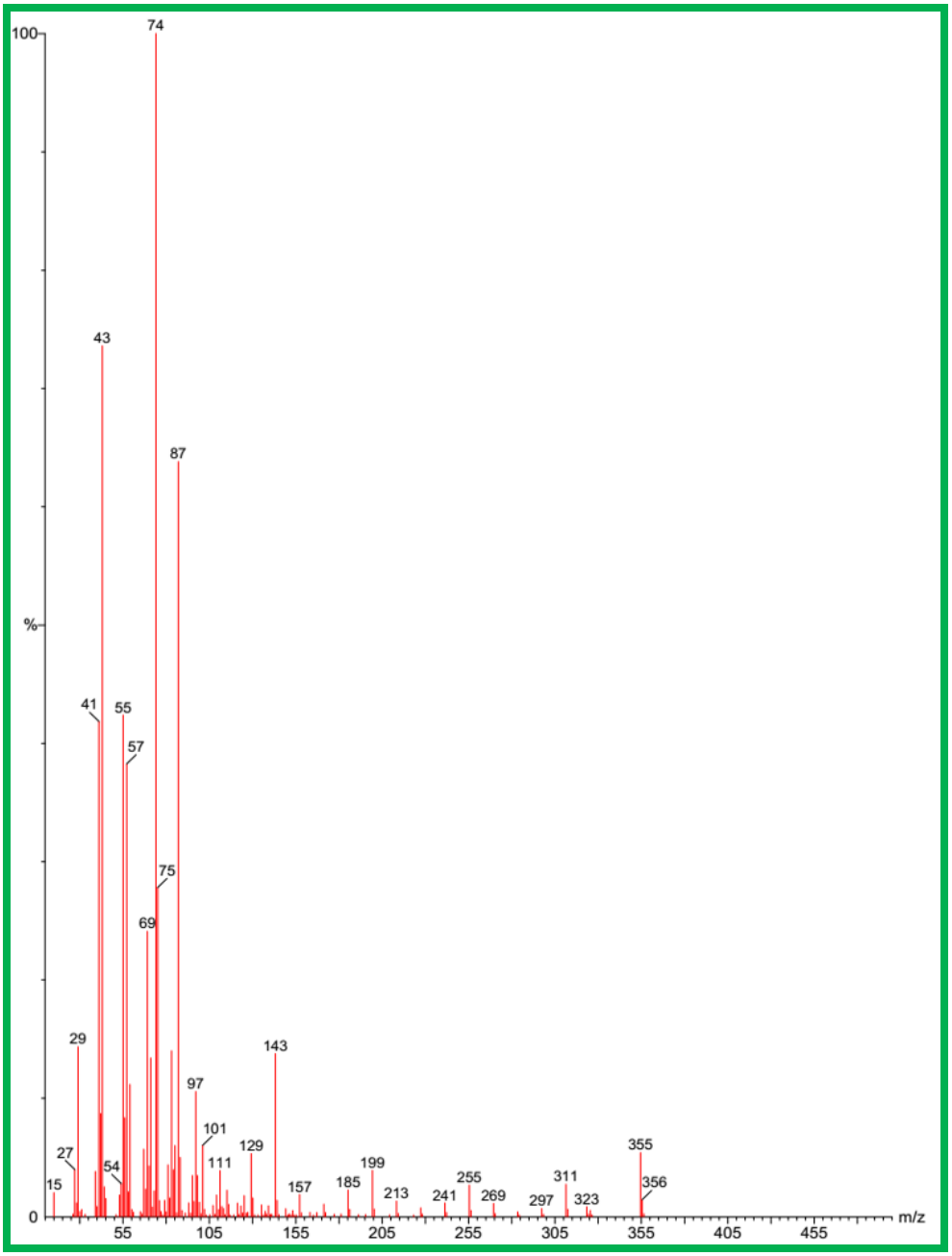

Figure 4.19 GC-MS spectrum of behenic acid, methyl ester

4.3 Fish oil extraction

Waste fish oil extracted from the discarded parts (viscera, eyes, fines, tails and maw as shown in Figure 4.20) of fish species *Cirrhinus mrigala, Cirrhinus cirrhosa and Cirrhinus reba* were collected from local fish market from Varanasi, India. The collected parts of fish were washed with hot distilled water to remove blood and solid particles associated with them. Thereafter, discarded parts were kept in a hot air oven at 102 °C for 70 min to remove water content. These dried discorded parts of fish were cut into small pieces and waste fish oil was extracted from these small pieces through mechanical expeller followed by solvent extraction using petroleum ether as solvent. Physical and chemical properties of extracted waste fish oil were determined (Table 4.6) and used as feedstock for the synthesis of biodiesel.

Figure 4.20 Represents the discarded parts of fish.

Table 4.6 Physical and chemical properties of waste fish oil.

Property	Unit	ASTM Standards	Value
Color	-		Yellowish red
Acid value	mg KOH/g	ASTM D 664	11.80
Unsaponifiable matter	% w/w	ASTM D1065	0.78
Density at 15.5 °C	g/cm^3	ASTM D 1298	0.891
Boiling point	°C	-	> 356
Cloud point	°C	ASTM D 1510	5
Saponification value	mg KOH/g		187
Pour point	°C	ASTM D 97	3
Kinematic viscosity, at 40 °C	mm^2/s	ASTM D 445	25.51
Flash point	°C	ASTM D 93	211
Water content	in%	ASTM D 2709	0.009%
Copper strip corrosion	3h/50 °C	ASTM D 130	No Corrosion observed

4.3.1 Characterization of fish oil extraction

4.3.1.1 Gas Chromatography–Mass Spectrometry (GC-MS) analysis of waste fish oil

Fatty acid composition of the waste fish oil was determined by using Gas Chromatography Mass Spectrometry. Waste fish oil sample was prepared according to above mentioned method (Section 4.2.1.1, Chapter 4) for the GC-MS analysis. Figure 4.21 represents the GC-MS chromatogram of waste fish oil in which X axis and Y axis represented the retention time and parentage of relative abundance. Fatty acid

composition present in the waste fish oil were predicted by using NIST 2011 library with help of Turbo Mass software. Fatty acid composition present in the waste fish oil were Myristic acid methyl ester (Figure 4.22), Palmitoleic acid methyl ester (Figure 4.23), Palmitic acid methyl ester (Figure 4.24), Arachidonic acid methyl ester (Figure 4.25), Oleic acid methyl ester (Figure 4.26), Linoleic acid methyl ester (Figure 4.27), Stearic acid methyl ester (Figure 4.28), Eicosapentaenoic acid methyl ester (EPA) (Figure 4.29), Docosahexaenoic acid methyl ester (DHA) (Figure 4.30) and Erucic acid methyl ester (Figure 4.31) as shown in Table 4.7.

Table 4.7 Fatty acid composition (%) of waste fish oil.

Sr.	Retention time	Compound name	Composition (%)	Corresponding fatty acid	Corresponding fatty acid strucure
1	17.37	Myristic acid methyl ester	5.51	Myristic acid	$CH_3(CH_2)_{12}COOH$
2	19.32	Palmitoleic acid methyl ester	9.70	Palmitoleic acid	$CH_3(CH_2)_5CH=CH(CH_2)_7COOH$
3	19.55	Palmitic acid methyl ester	14.09	Palmitic acid	$CH_3(CH2)_{12}COOH$
4	21.06	Arachidonic acid methyl ester	3.21	Arachidonic acid	$CH_3(CH_2)_{10}(CH=CH)_4COOH$
5	21.25	Oleic acid methyl ester	11.03	Oleic acid	$CH_3(CH2)_{14}CH=CHCOOH$
6	21.29	Linoleic acid methyl ester	3.45	Linoleic acid	$CH3(CH2)_{10}(CH=CH)_3COOH$
7	21.46	Stearic acid methyl ester	4.05	Stearic acid	$CH_3(CH2)_{16}COOH$
8	22.77	Eicosapentaenoic acid methyl ester (EPA)	19.96	Eicosapentaenoic acid	$CH_3(CH_2)_8(CH=CH)_5COOH$
9	24.33	Docosahexaenoic acid methyl ester (DHA)	13.93	Docosahexaenoic acid	$CH_3(CH_2)_8(CH=CH)_6COOH$
10	24.66	Erucic acid methyl ester	1.08	Erucic acid	$CH_3(CH_2)_{18}(CH=CH)COOH$

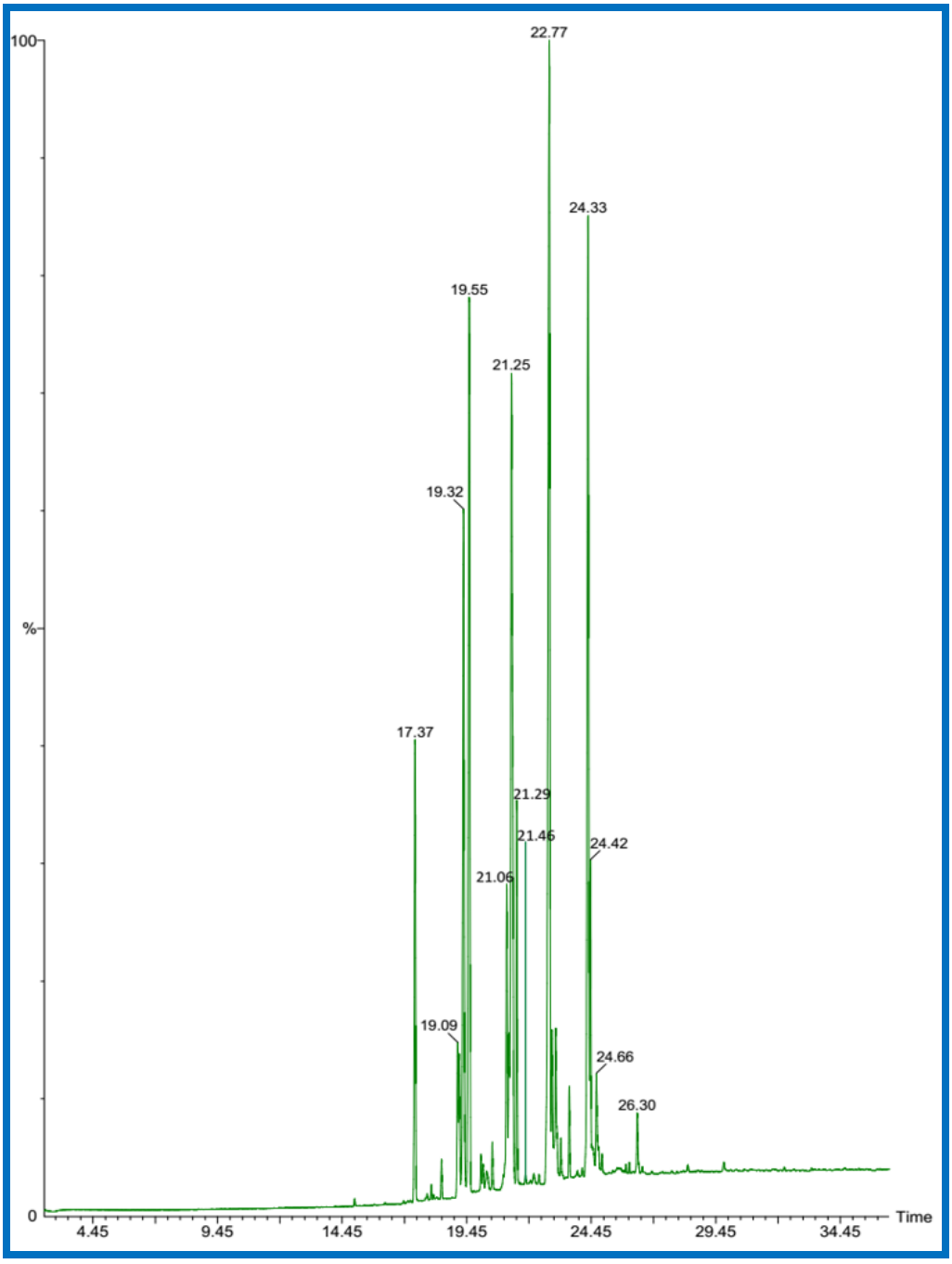

Figure 4.21 GC-MS chromatogram of waste fish oil.

.

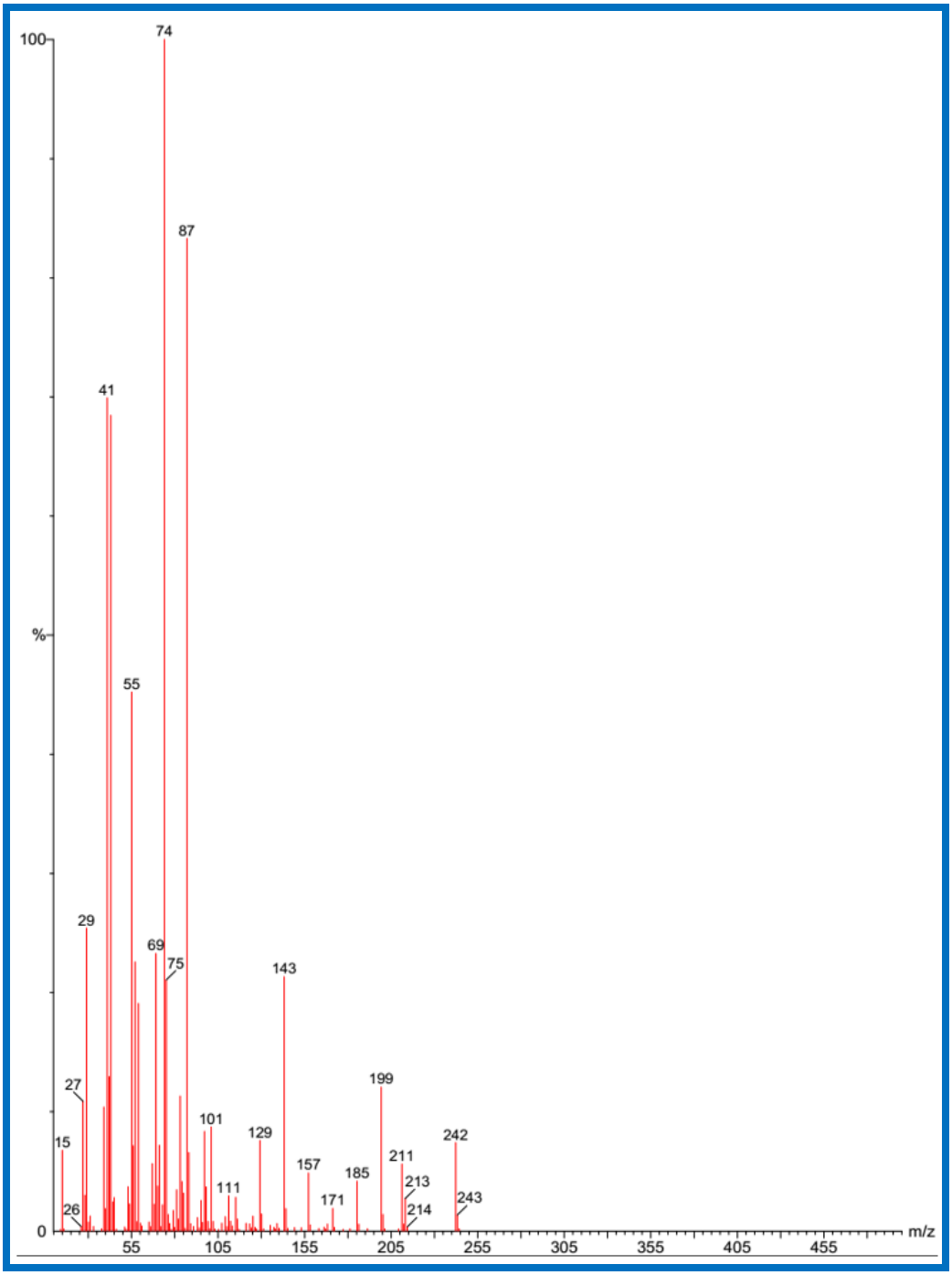

Figure 4.22 GC-MS spectrum of myristic acid methyl ester.

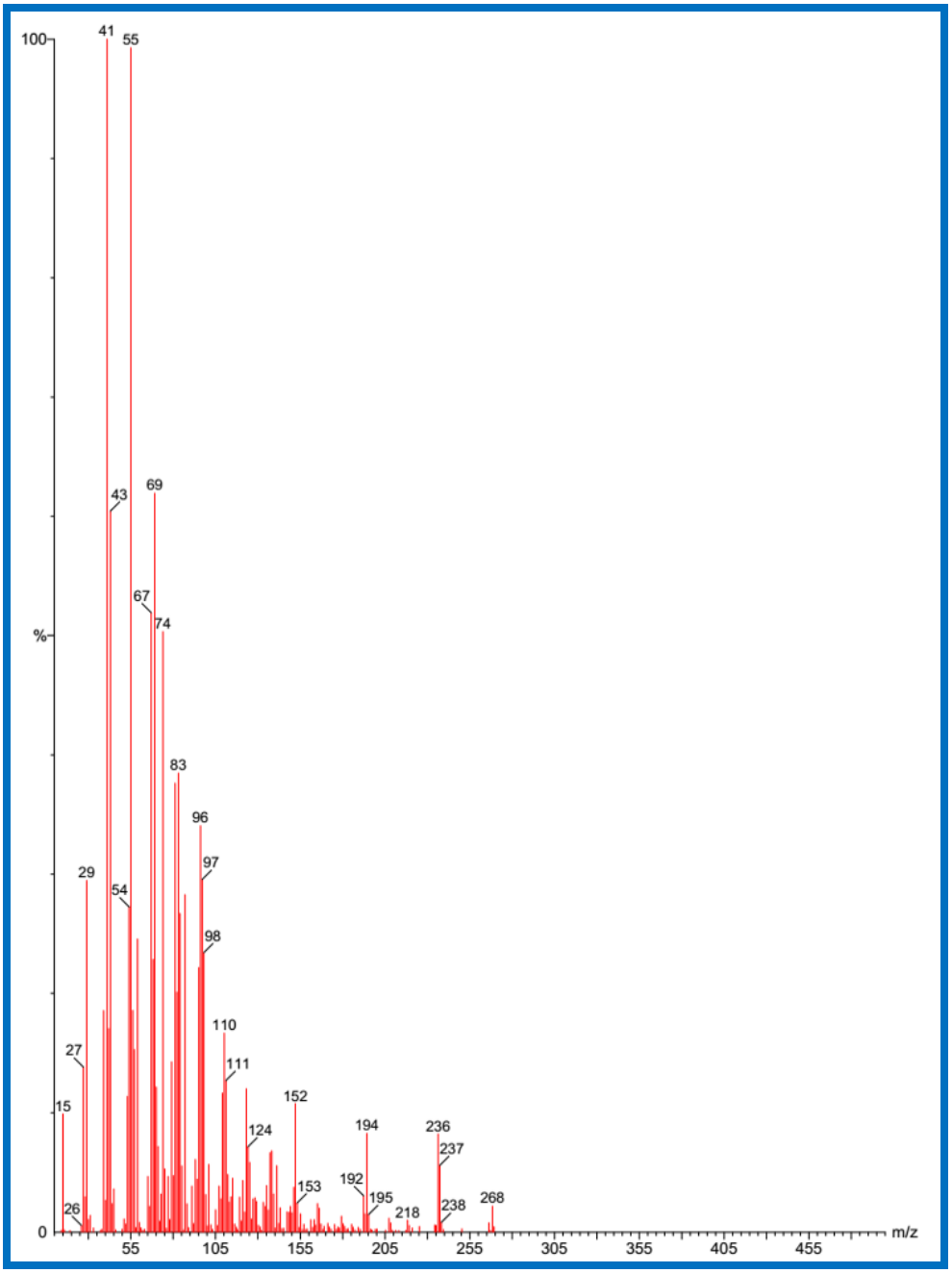

Figure 4.23 GC-MS spectrum of palmitoleic acid methyl ester.

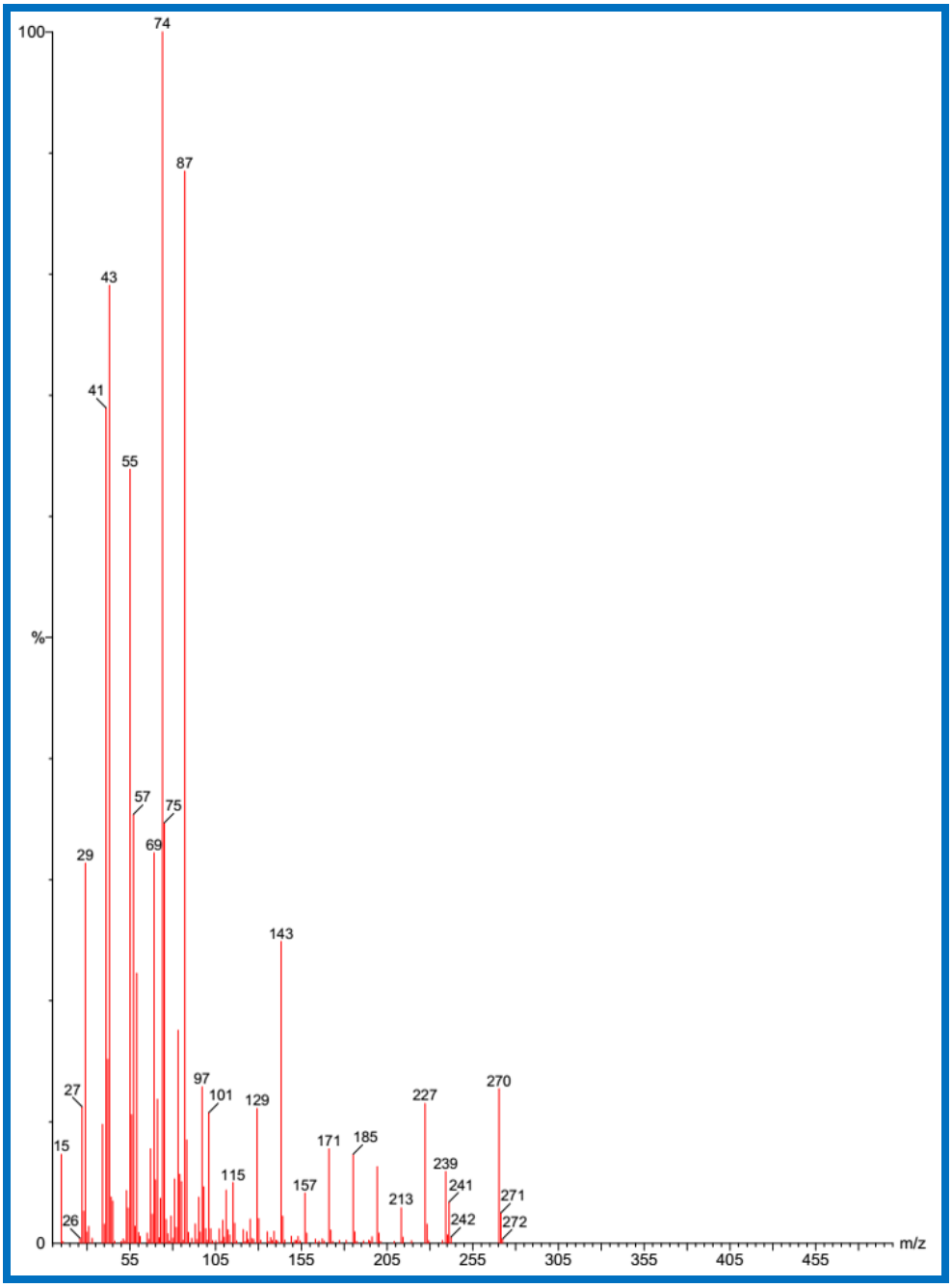

Figure 4.24 GC-MS spectrum of palmitic acid methyl ester.

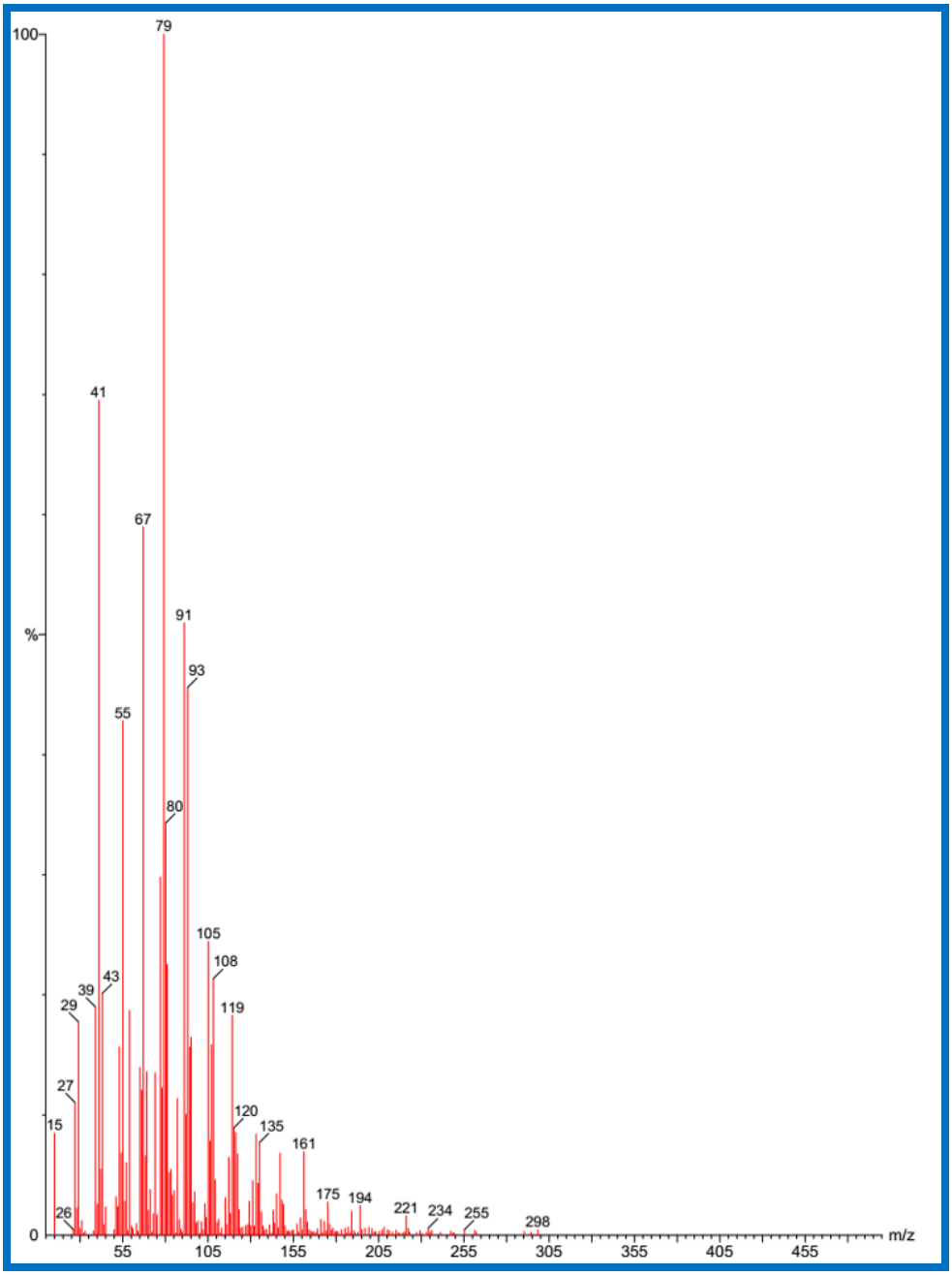

Figure 4.25 GC-MS spectrum of arachidonic acid methyl ester.

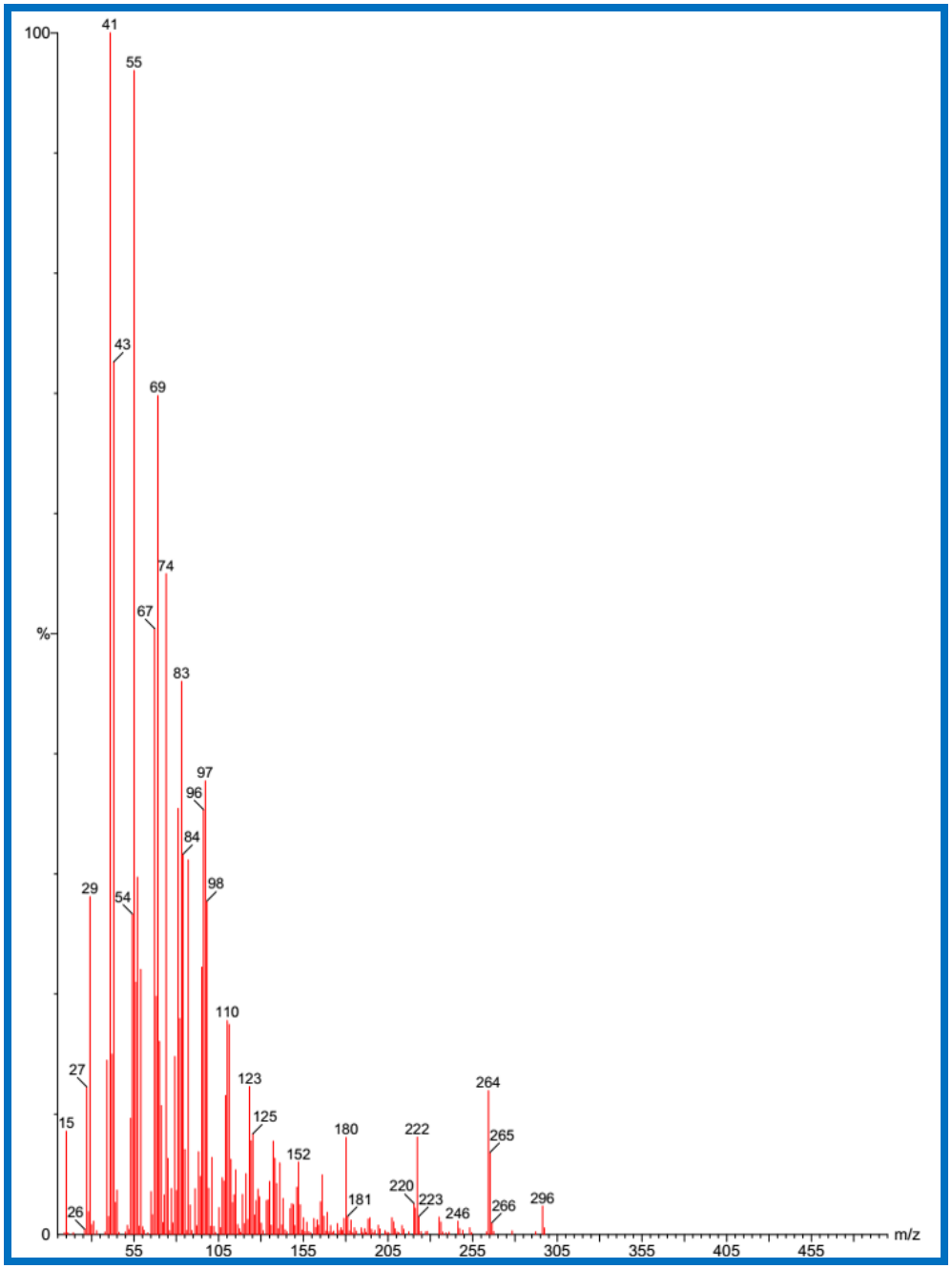

Figure 4.26 GC-MS spectrum of oleic acid methyl ester

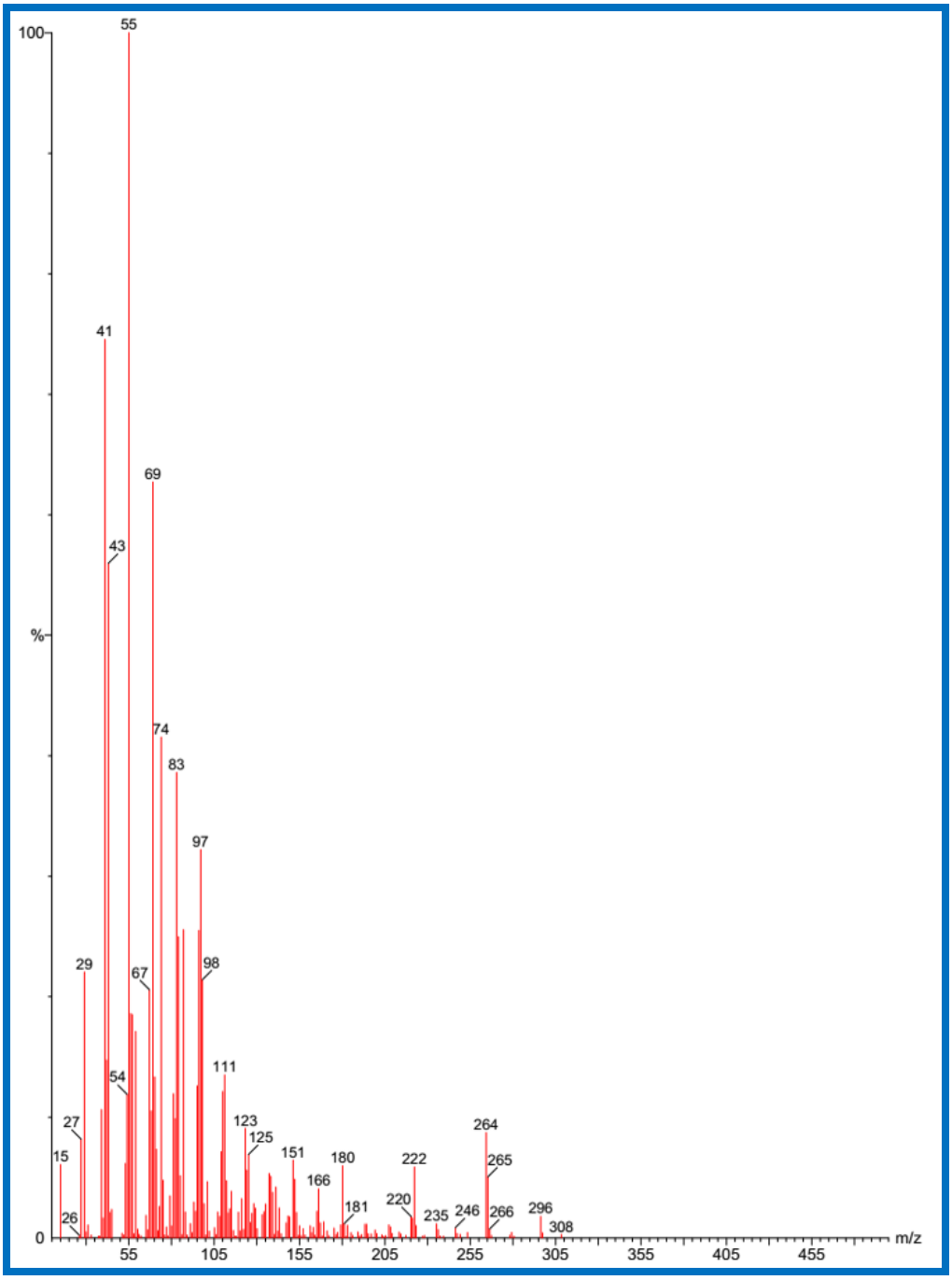

Figure 4.27 GC-MS spectrum of linoleic acid methyl ester.

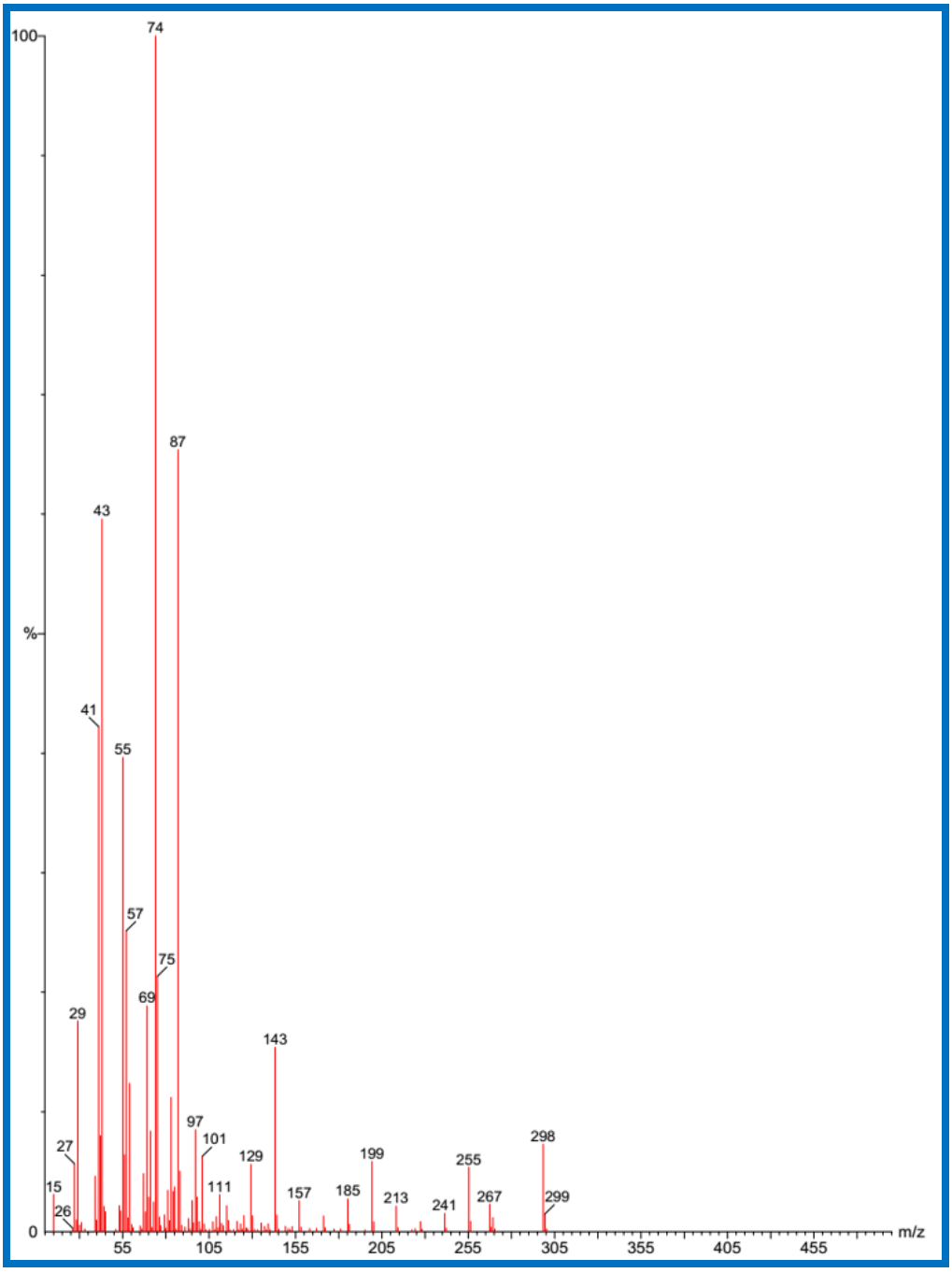

Figure 4.28 GC-MS spectrum of stearic acid methyl ester.

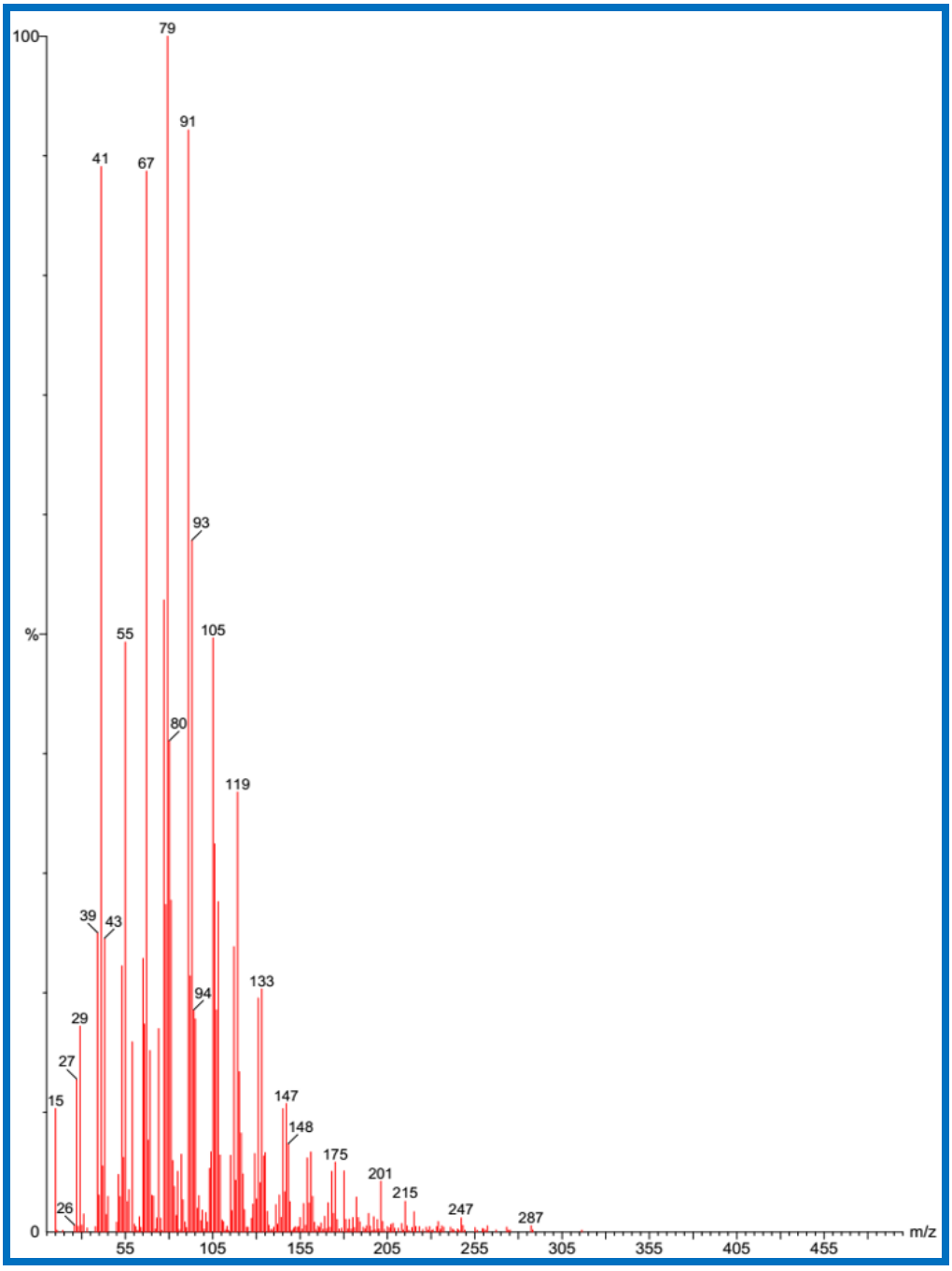

Figure 4.29 GC-MS spectrum of eicosapentaenoic acid methyl ester (EPA).

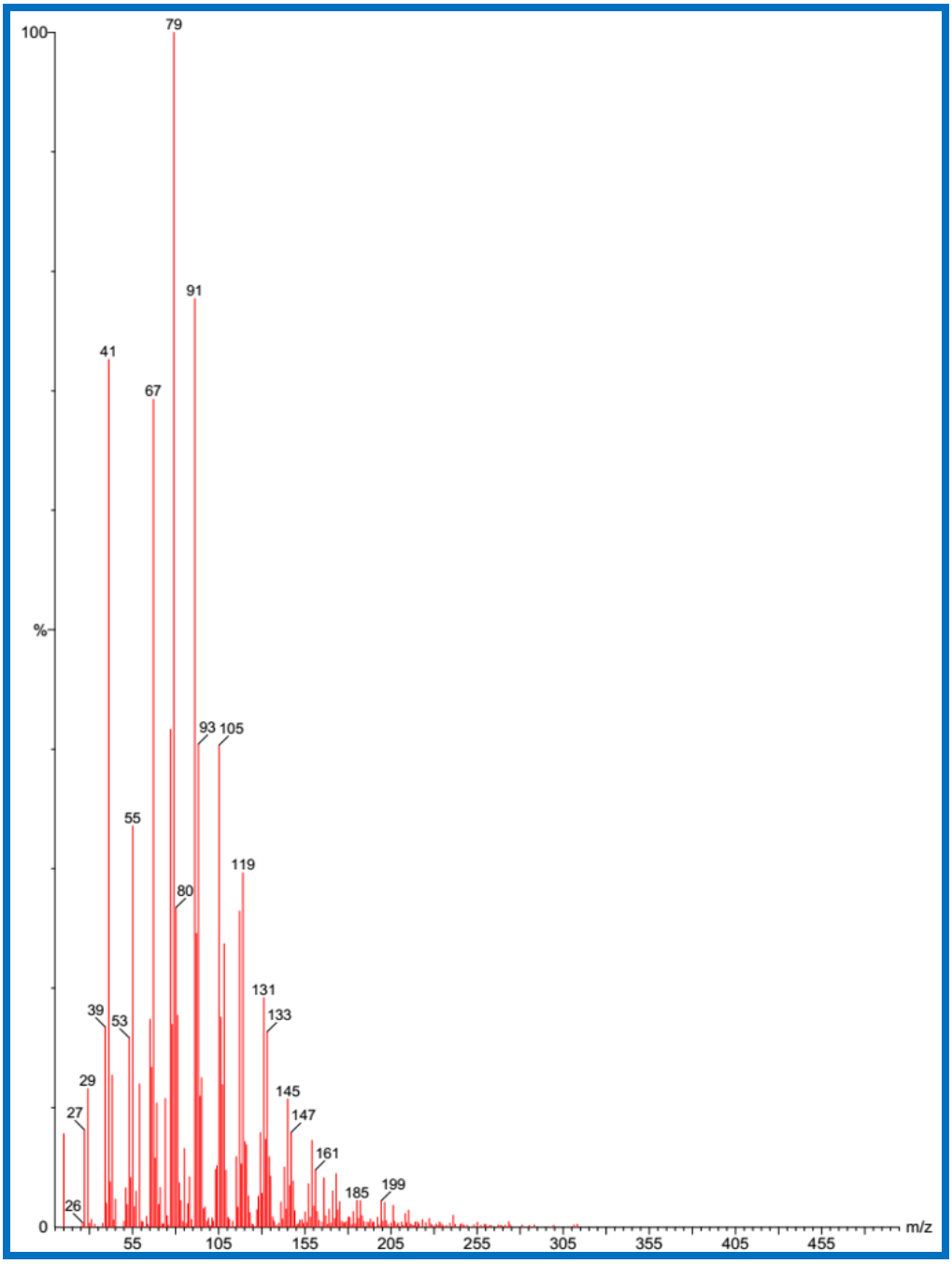

Figure 4.30 GC-MS spectrum of docosahexaenoic acid methyl ester (DHA).

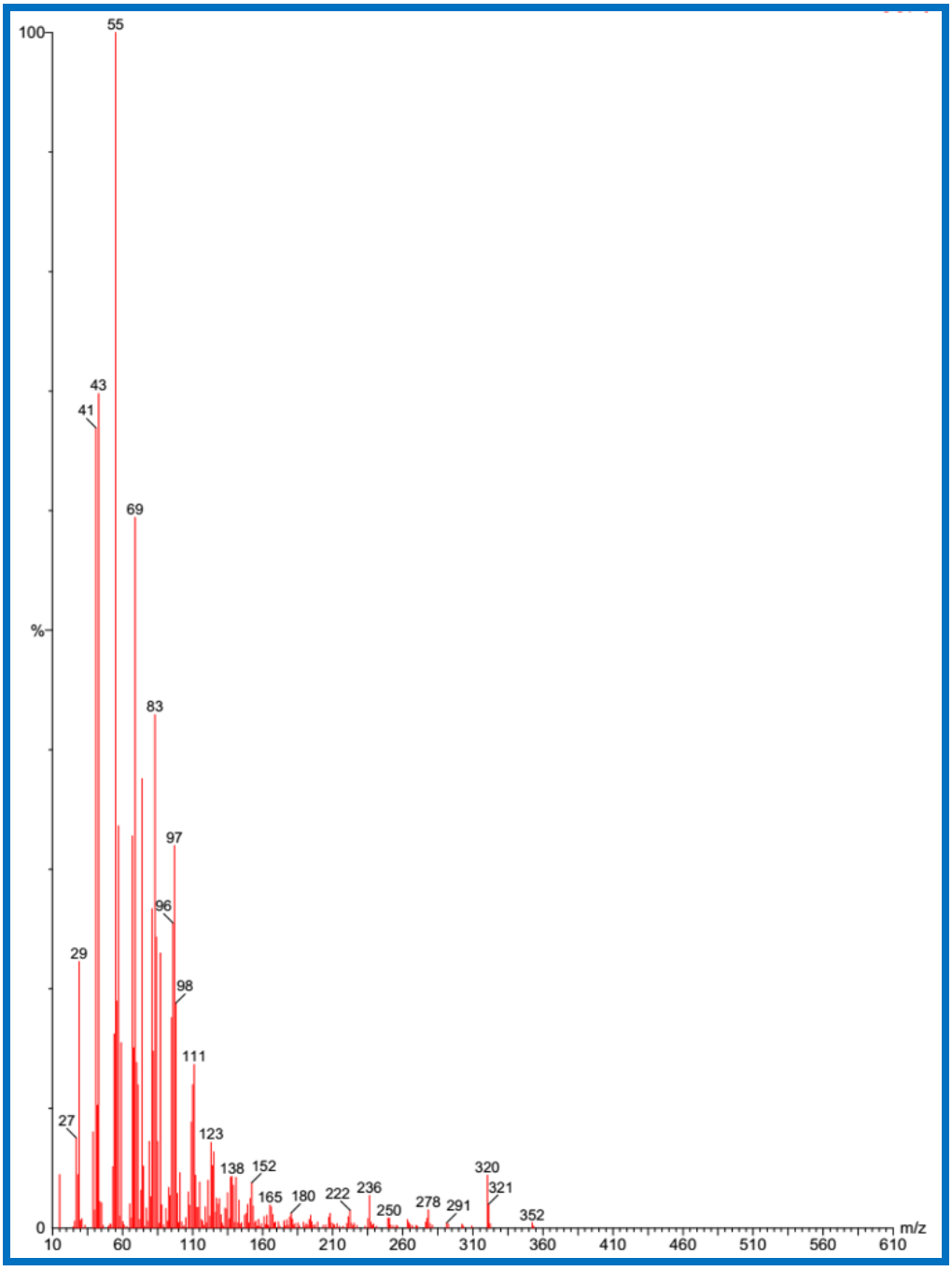

Figure 4.31 GC-MS spectrum of erucic acid methyl ester.